ESI - Supplemental Information

for

Development of Continuous Spatially Distributed Diafiltration Unit Operations

Zoheb Khan[abd*], Xiaoyan Long[ad*], Eoin Casey[a], Denis Dowling[c], Steven Ferguson[abde]

[a]*School of Chemical and Bioprocess Engineering, University College Dublin, Belfield, Dublin 4.*

[b]*I-form, the SFI Research Centre for Advanced Manufacturing, School of Chemical and Bioprocess Engineering, University College Dublin, Belfield, Dublin 4*

[c]*I-form, the SFI Research Centre for Advanced Manufacturing, School of Mechanical and Materials Engineering, University College Dublin, Belfield, Dublin 4*

[d]*SSPC, the SFI Research Centre for Pharmaceuticals, School of Chemical and Bioprocess Engineering, University College Dublin, Belfield, Dublin 4*

[e]*National Institute for Bioprocess Research and Training, 24 Foster's Ave, Belfield, Blackrock, Co. Dublin, A94 X099, Ireland*

**These authors contributed equally to this study*

1.1 System stability

Samples collected from rejection test as described in section 3.5.2. Three samples are collected for each test after membrane performance reaching a steady state, and the rejection coefficient test is repeated three times for different pieces of membrane. Figure S1 illustrates the ibuprofen and ethanol rejection coefficient for the DuraMem-150 at an operating flow rate 5 mL/min and transmembrane pressure of 55 bar. Due to the variability in the performance of the commercial OSN membrane, the rejection coefficient of ibuprofen and ethanol were 90% ± 2% and 8% ± 3%, respectively. The graph shows the stable system performance when the membrane separated ethanol from ibuprofen-methanol solution. Therefore, this system could be adopted to the following diafiltration experiment for the concept verification and comparison.

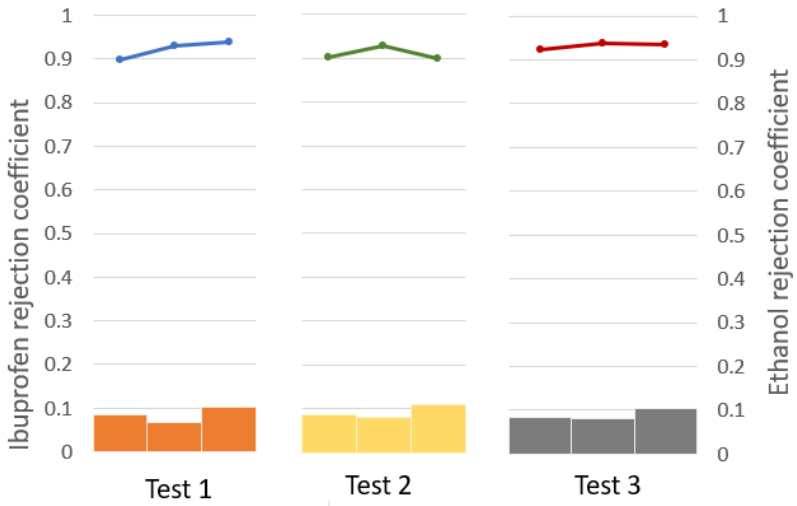

Figure S1 Ibuprofen-ethanol-Methanol separation performance stability with DuraMem-150

1.2 Permeability test

The membrane permeability was found to be $0.0001547 \pm 1.67 \times 10^{-5}$ L/(m^2h bar) ($R^2 = 0.996$). As shown in Figure S2, the ibuprofen rejection coefficient of ibuprofen was relatively stable from 15 bar to 55 bar, but the ethanol rejection coefficient is slightly decreased with decreased membrane channel pressure. Therefore, all the following diafiltration experiments were investigated under 55 bar of transmembrane pressure for consistent chemical rejection coefficient and higher permeate flux.

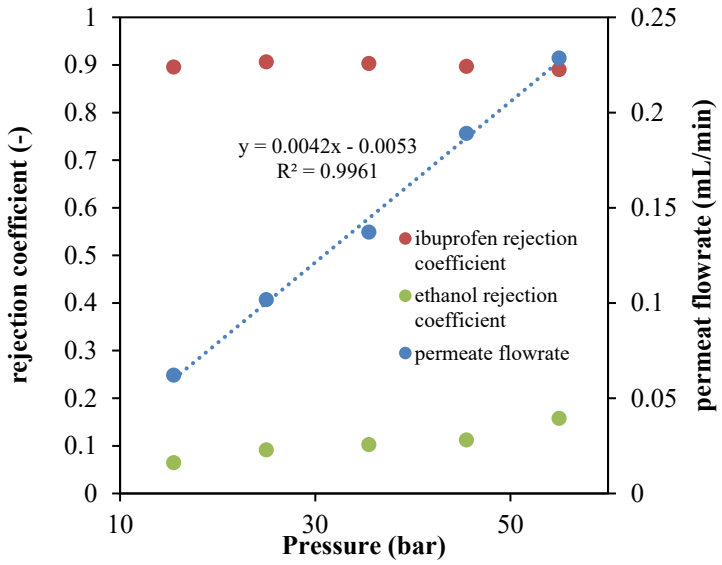

Figure S2 Rejection coefficient and permeate flowrate with different transmembrane pressure

2. Mixer Design

Two configurations were chosen; a serpentine formation allowing for a longer residence time with the secondary solute being injected from the top intermittently to accelerate the flow and a straight channel flow with mixers running along the length with the secondary solute injected from above. The mixers were printed along with supports that fit into the rig as a single piece allowing for the rig to be used for multiple applications by simply switching the mixer unit. Figure S3 shows a 3D printed mixer unit incorporating the kinecs static mixer. The alternating segments are connected via a narrow strip to provide structural stability at the time of printing and overcome the problem of overhangs.

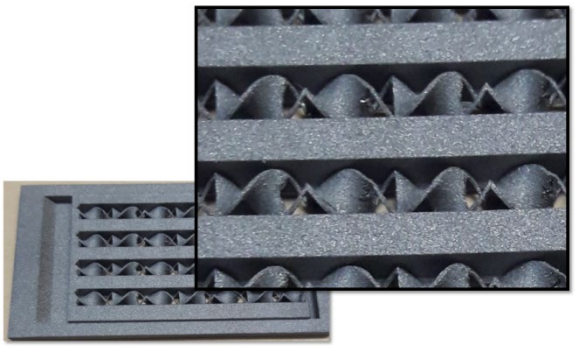

Figure S3. 3D printed mixer unit with kinecs static mixers.

The serpentine setup is shown in Figure S4. The serpentine channel was designed to have a arching shape at the top to allow ease of printing and structural stability. The pathway of the flow has intermittent ridges that allow for the suspension of the flow and inlet points that impinge the secondary solute on the membrane serving a dual purpose of mitigation of concentration polarization layer and the mixing of the two solutes.

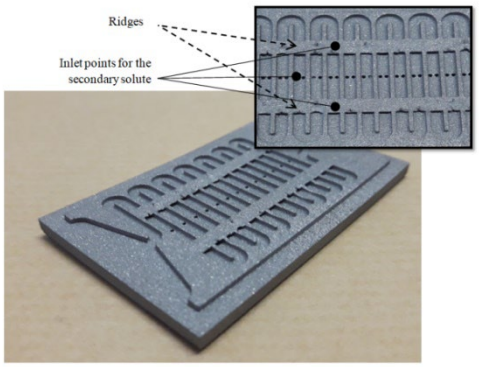

Figure S4. Serpentine setup, ridges allow for suspension of the solute, secondary solute enters through the inlets.

3. Mixer Flow Strategies

3.1 Concentration Polarization

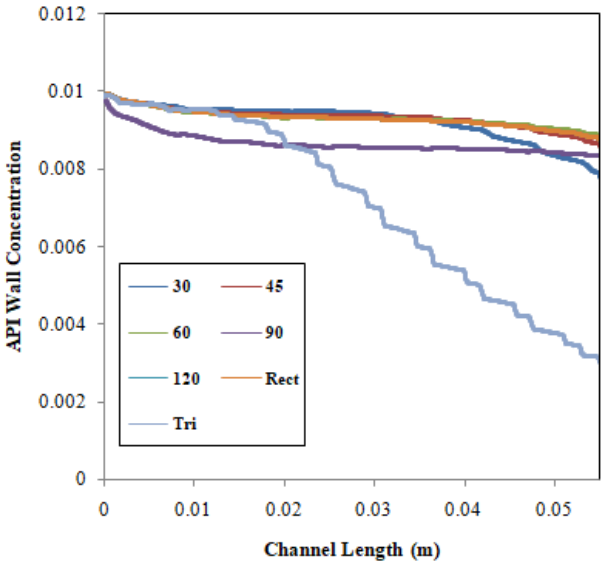

Figure S5. Wall concentration for different CS3D geometries

The solute concentration at the wall is found to be rapidly decreasing along the channel length. The objective of back-mixing the solute API seems to work with the splitting and recombining of the flow streams and also hydrodynamic focussing in case of the geometries with protrusions placed in the flow path.

3.2 Segmentation

The CS2D and CS3D concept segments the process of spatial diafiltration over a single membrane channel as observed in Figure S6. The segmentation results in smaller units of diafiltration and buffer exchange, increasing the overall permeate flux and hence reducing concentration polarization. Figure S6 illustrates the influence of the segments along the membrane channel length in a serpentine type of mixer. The microsolute concentration reduces in steps as observed in Figure S6 (c) and in its contours on a plane halfway up from membrane surface while the permeation flux proportionally increases in steps as well.

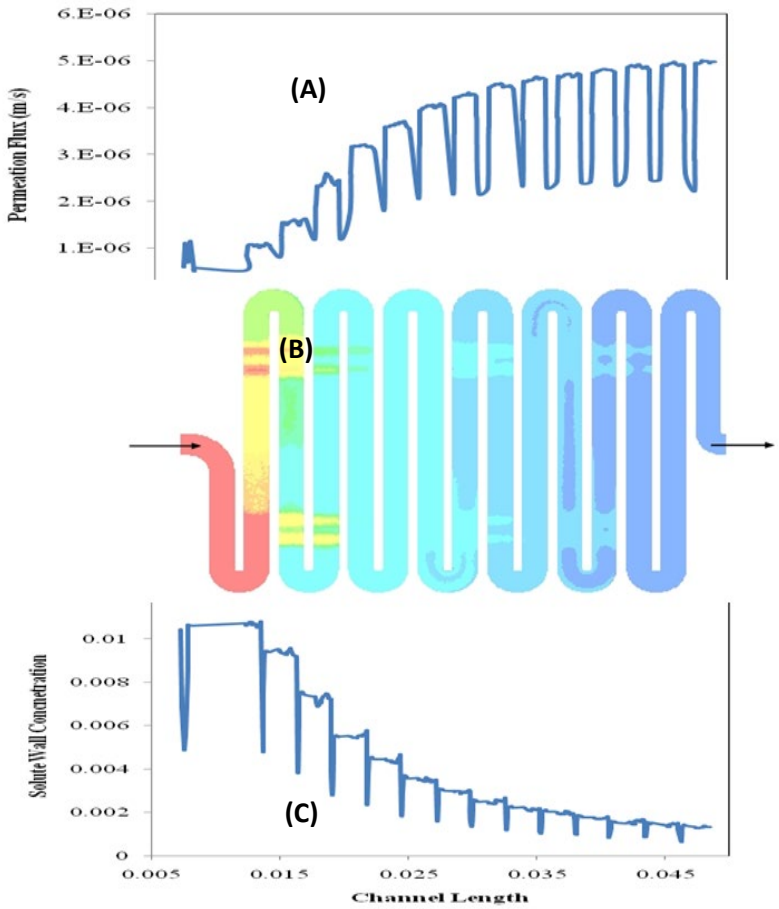

Figure S6. Distribution of the microsolute concentration over the membrane surface with the microsolute wall concentration and permeate flux overlayed.

3.3 Downflow Configuration

The mixer is fitted with a small gap preventing it from resting on the surface on the membrane bed, this allows a thin laminar layer to develop hence preventing the development of the concentration polarization layer. Figure S7 (A) and (B) shows the underside of the mixer. Lateral mixing is observed because of the gap between the mixer and the membrane, which allows for mixing along the length of the flow as transverse direction. It is also observed in figure 6 (b) that the flow is unaffected by presence of the supports. The folding and mixing characteristic of the kinecs mixer remains unperturbed.

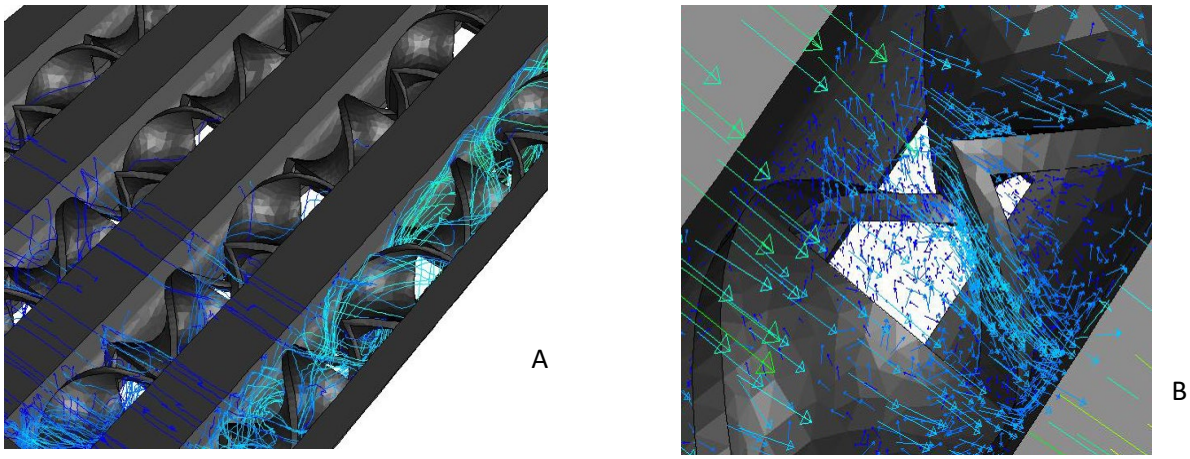

Figure S7: (A) Lateral flow observed transverse to the flow direction (B) rotational flow uninterrupted by the geometry modifications

3.4 Influence of the supporting walls

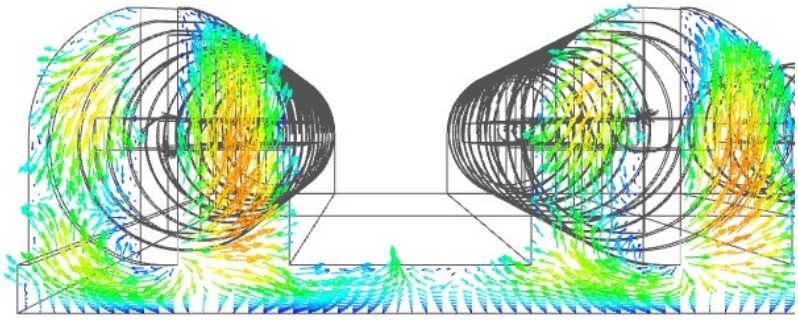

Figure S8: Flow vectors between adjacent mixer segments along the length of the membrane channel

Figure S8 illustrates the nature of the rotational flow between two segments of the mixer along the length of the channel separated by the supporting walls. The supporting walls provide support to the mixers to facilitate 3D printing. Minimal mixing is observed under walls supporting and separating the mixers, the strong rotational flow of the could aid lateral mixing in the absence of the walls and further mitigate the presence of polarization concentration in the channel.

3.5 Continuous Spatially Distributed Diafiltration Mixer Design

Section 2 outlines the expected performance for continuous spatially distributed diafiltration

at the extremes of performance under idealized mixing conditions. However, the ability to achieve such performance in real fluid flows requires the development of mixers to facilitate approximation of the idealized operations previously discussed (Section ESI, Section 2 can be fabricated with complex geometries via 3D printing, although this still imposes some specific geometric constraints. (ESI Section 3)

Mixers of different characteristics are developed and printed as shown in ESI, Section 3. Some of them are based upon commonly used static mixers employed in industry and all are simulated and modified to better suit the concept of continuous spatially distributed diafiltration. For example Kinecs, SMX, and KMX-V mixers have been simulated, and though these mixers are commonly employed in the circular pipes, they have been simulated within a rectangular channel in this case. The rectangular channels are then placed adjacent to each other along the width of the channel to span the entire membrane permeation area, as they would be configured in the fabricated device. The operating channel dimensions are 30mm (W) by 55 mm (L) by 3mm (H), with each segment housing the mixer 3mm (W) by 55 mm (L) by 3 mm (H).

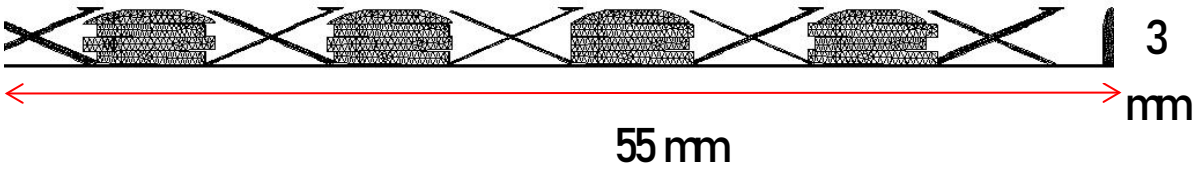

Figure S9. Side view of a meshed SMX mixer with height and length of the domain.

Figure3 illustrates the meshed domain of a rectangular segment with the channel housing an SMX mixer. The triangulations appearing on the mixers are the surface meshes. The domain volume cells are hidden to display the placement of the static mixers.

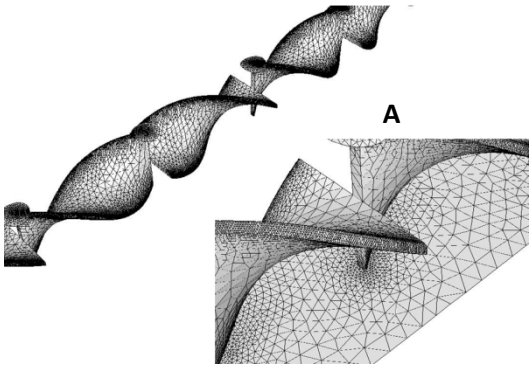

Figure S10. Surface mesh for the Kinecs mixer (A) unstructured surface mesh (B) a closer look at the surface mesh; increase in skewness at the points of contact of independent surfaces

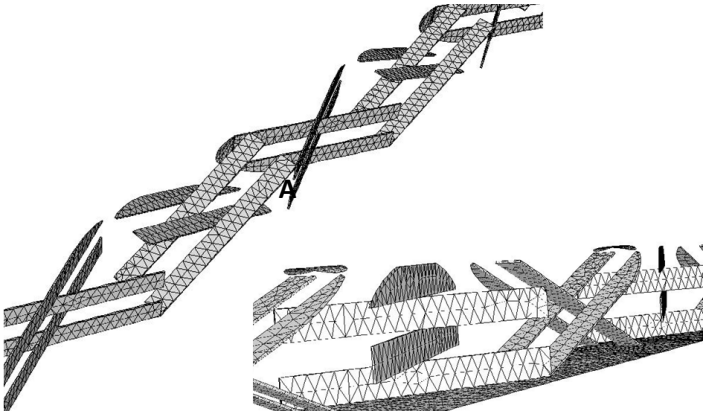

Figure S11. Surface mesh of the SMX mixer within a rectangular segment with the membrane channel

Figure S10 and Figure S11 illustrate the surface mesh on the static mixers within the rectangular segment inside the membrane channel unit. The simulation domain is hexahedral dominant with an average skewness of 0.78 for the SMX mixer unit and 0.83 for the Kinecs mixer unit. The skewness increases at the points of the contact between two surfaces with lowest skewness value of 0.64, allowing the simulation to converge safely. An inflation layer composing of 12 layers of cells have been stacked; with an increment factor of 1.3, from the boundary surface to the bulk of the flow. The simulation domain is created with by a Boolean subtraction between the rectangular flow domain and the solid static mixer, this reduces the computational load when meshing the flow domain. With this approach there is no static mixer inside the flow domain but only its surface treated as a no-slip

boundary.

3.5.1 Constant volume semi-batch diafiltration experimental performance

A rejection test was conducted before each batch experiment to check the membrane performance. The rejection coefficient of ibuprofen and ethanol were 88%, 89%, 87% and 17%, 16%, 15% respectively. The product was collected from the feed vessel at different diavolumes to measure the component concentrations and calculate the product purity and yield.

Figure S12 describes the purity and yield trend for up to 5 diavolumes, and Figure S13 shows the corresponding ibuprofen and ethanol concentration for the first 5 diavolumes. Based on Figure S12 and S13, the semi-batch diafiltration product yield decreased to 52% as the ibuprofen concentration dropped from 10 g/L to around 5.2 g/L. The product purity increased from 11% to 68% while the ethanol concentration decreased from 75 g/L to 2.4 g/L. 96.7% impurity was removed from API in the semi-batch diafiltration. Figure S14 revealed the permeate flux variation during the batch experiment, the permeate flux slightly raised with the increased number of diavolume as a results of decreased components concentration. Overall, the three semi-batch diafiltration experiments were shown to have a consistent performance and the average value was used to compare them with the continuous CS2D/CS3D experimental results.

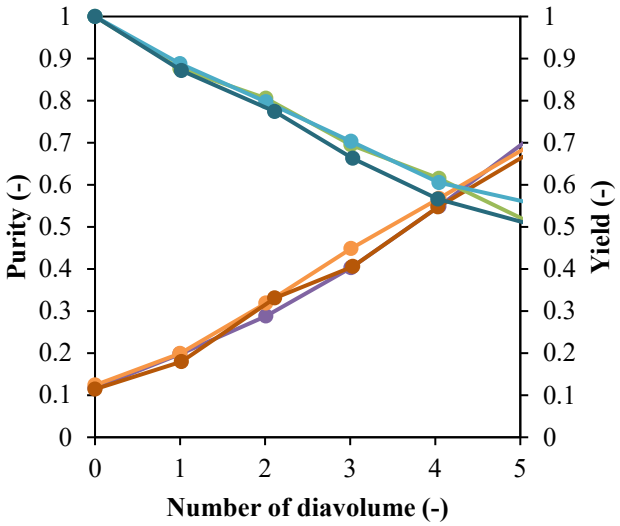

Figure S12. Purity and yield of Ibuprofen for different diavolumes in a constant volume semi-batch diafiltration system

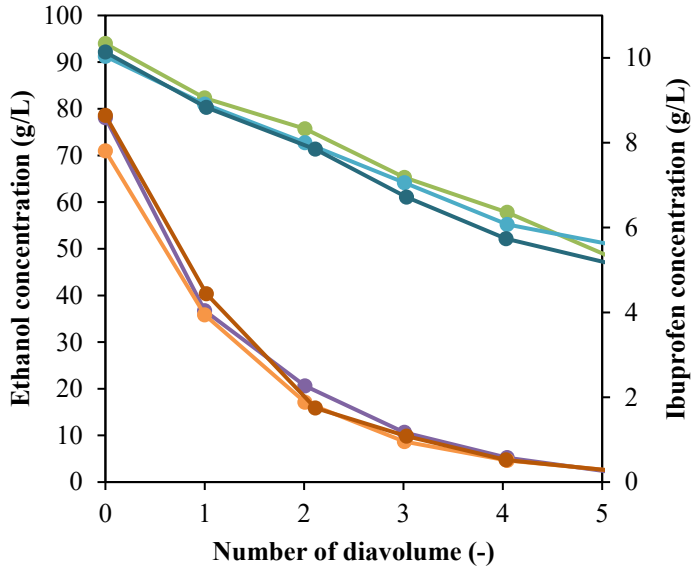

Figure S13. Comparison of Ethanol and Ibuprofen concentrations for different diavolumes in a constant volume semi-batch diafiltration setup.

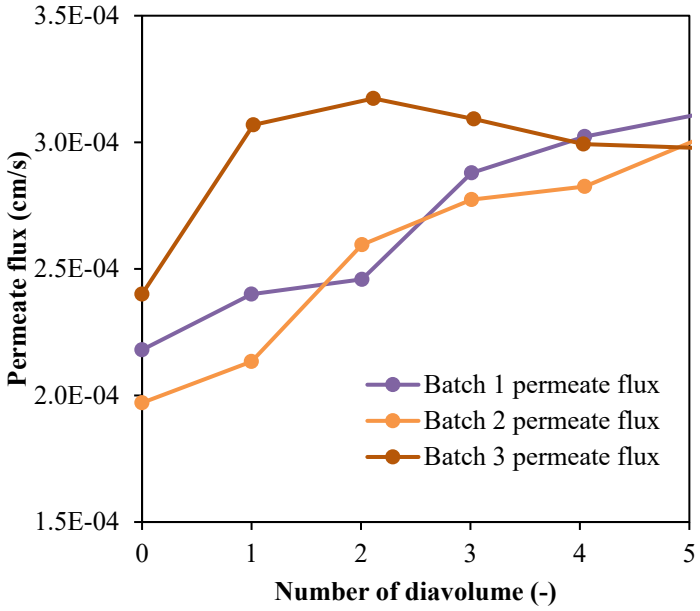

Figure *S*14. Comparison of permeate flux (cm/s) for three runs for constant volume semi-batch diafiltrations at different diavolumes.

3.6 CS3D mixer counter plots (Magnified Figure 5 from Manuscript Section 4.2)

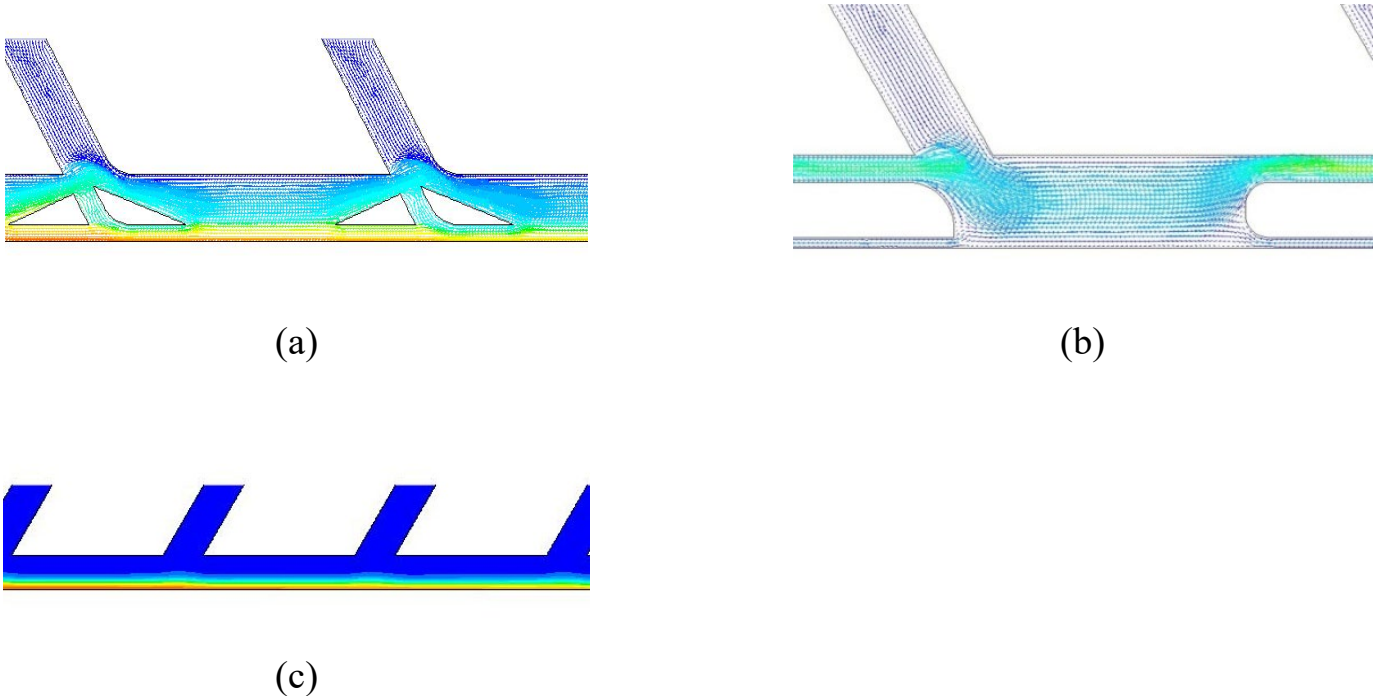

(a) (b)

(c)

Figure S15. Velocity vector and contour profiles for CS3D (a) Triangular obstacles (b) rectangular obstacles (c) reversed dilutant flow

3.7 Flow visualization and analysis, CS2D geometries

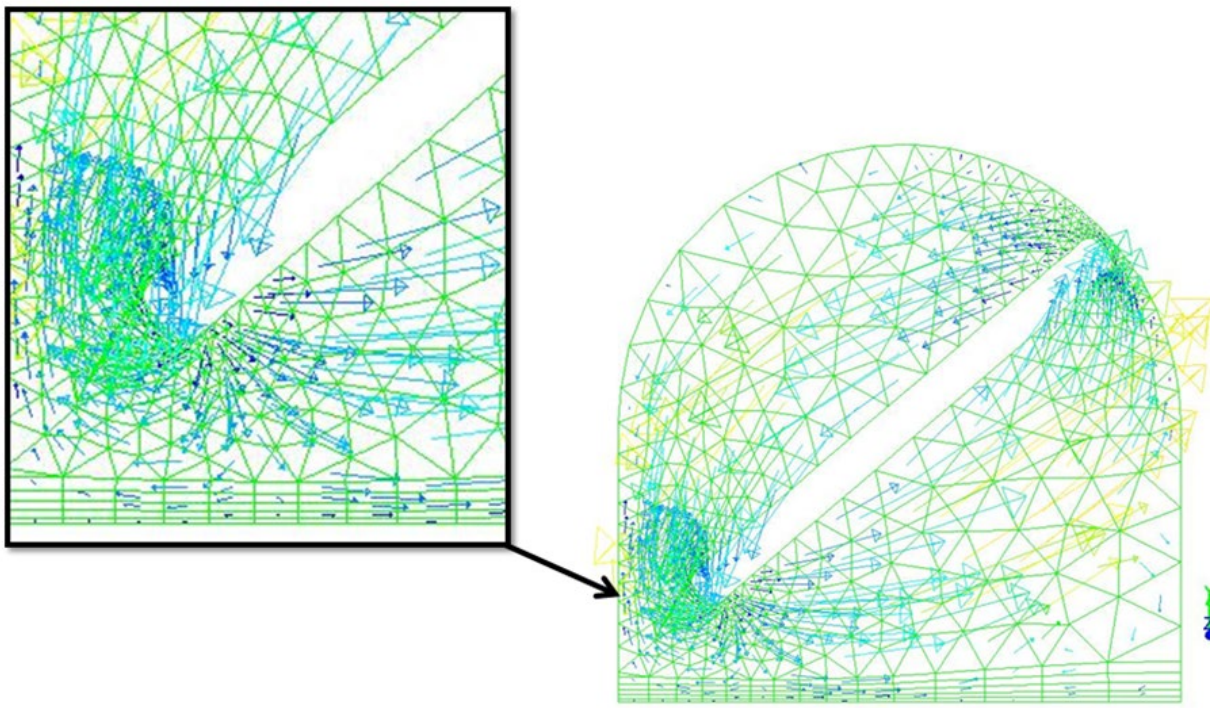

Figure S16. Front view cross section of one Kinecs mixer showing the rotational flow sweeping up flow off the membrane surface

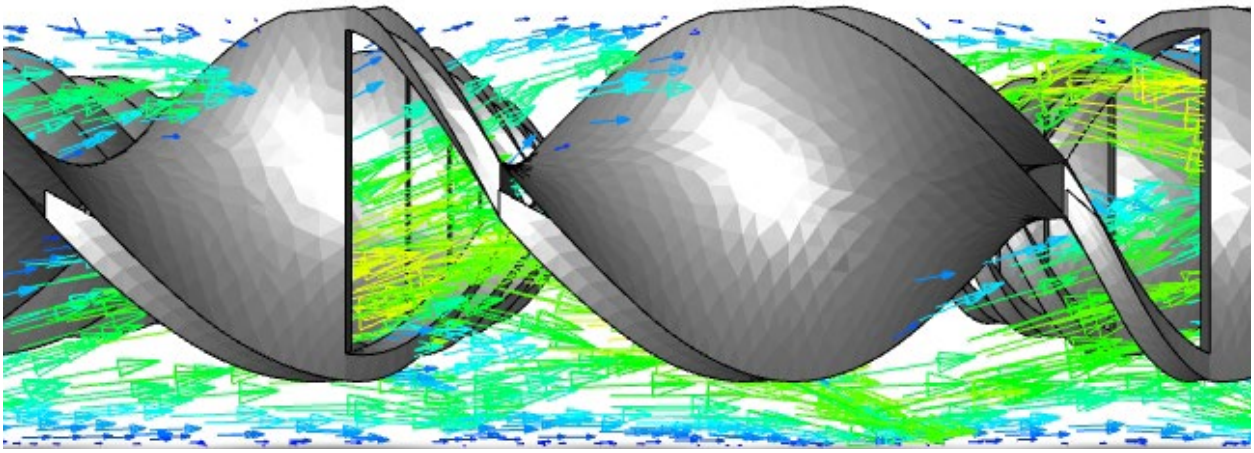

Figure S17. Absence of downstream vortices in the Kinecs type mixer segment

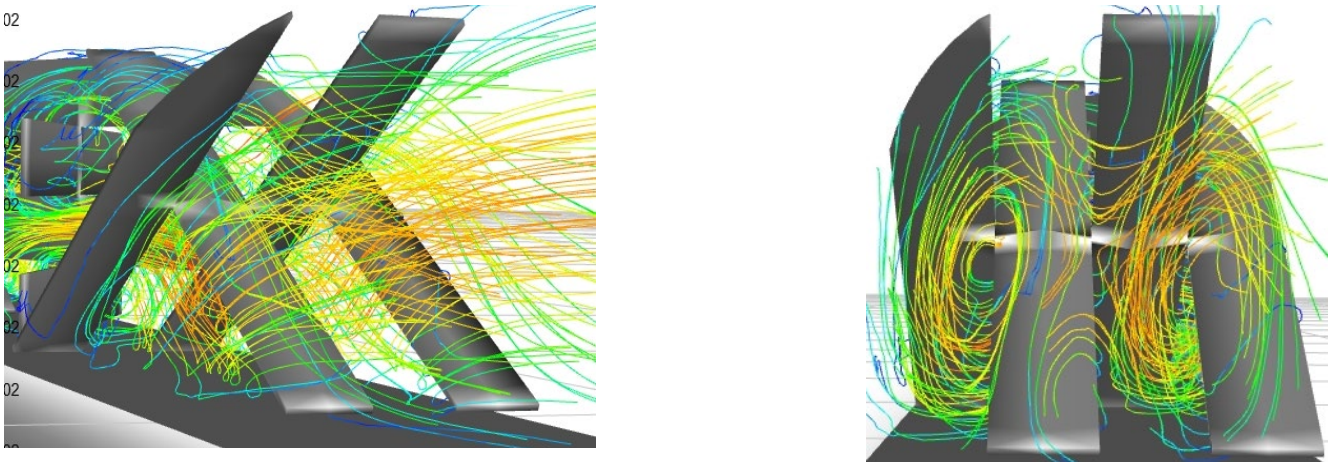

Figure S18. Strong dowstream vortexes along the flow path in the SMX mixer segment

3.8 CFD visualization of deviation real CSDD purification results from idealized CS2D/CS3D performance

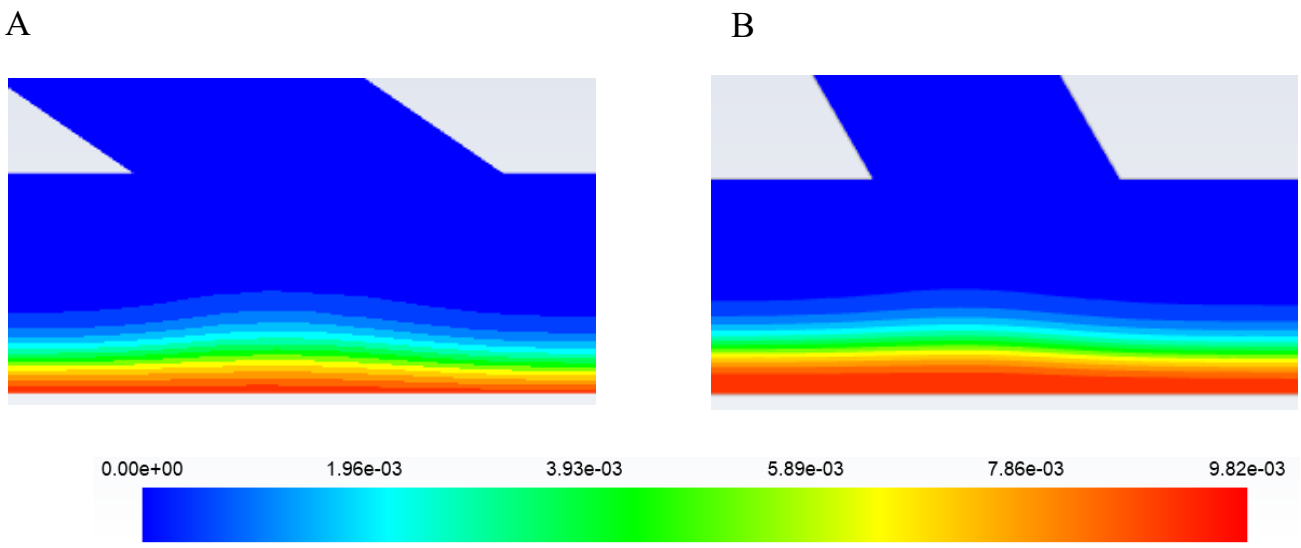

Figure S19. Comparison of the solute hold-up at the membrane interface in the CS3D scenario. (A) CS3D-30 (B) CS3D-60

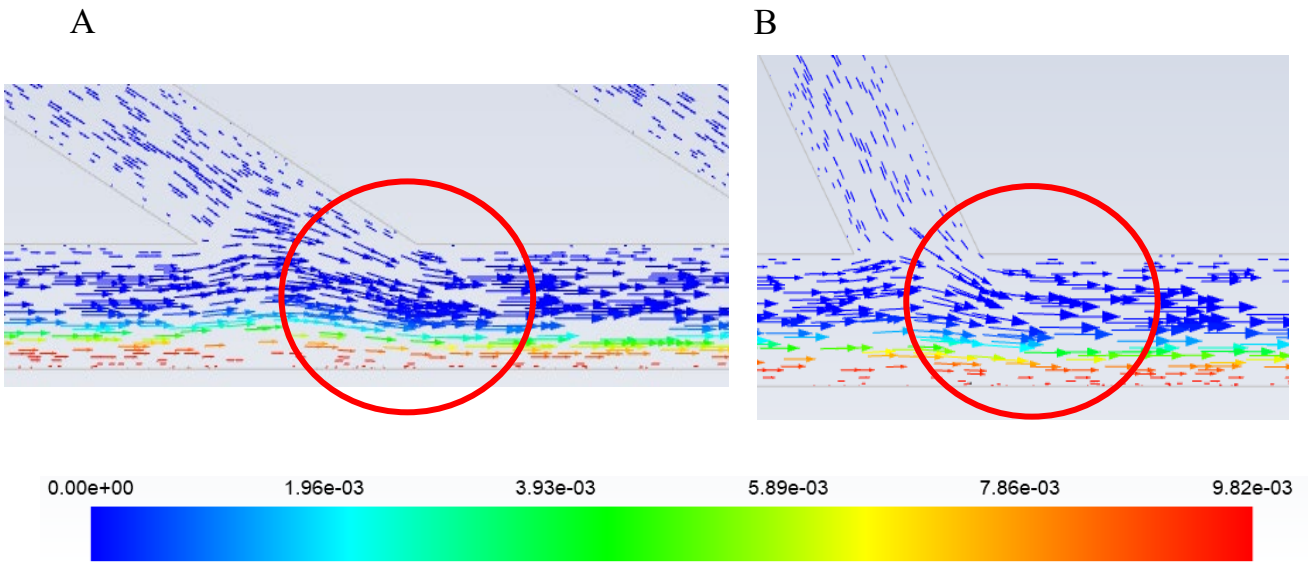

Figure S20. Comparison of the solute hold-up at the membrane interface in the CS3D scenario. (A) CS3D-30 (B) CS3D-60

4. Computational fluid dynamics and multiscale modeling

Investigation of the flow dynamics in relation to the polarization concentration in membrane channels with CFD have been emerging since the late 1990s [28]. Along with the numerical computation, implementation of experiments for predicting parameters and validation is of crucial necessity to avoid dependence on mass transfer modeling of semi-empirical correlations. A two-dimensional rectangular geometry is generated using commercial CFD package ANSYS. The solution domain was identical to the experimental setup of [40]; i.e. (l x h) 255mm x 1mm, and was used to verify the modeling assumptions and permeation flux model used in this study. A detailed description of the CFD modeling approach used in this study can be found here in Section 4 of the ESI for this manuscript.

4.1 Governing equations

The steady state governing equations for the fluid flow and scalar transport quantities are discretized and solved for a two-dimensional laminar flow in a channel.

Continuity equation

$$\frac{\partial(\rho u)}{\partial x}+\frac{\partial(\rho v)}{\partial y}=0 \tag{5}$$

In the case of an incompressible laminar flow, the Navier-Stokes's equations govern the hydrodynamics. The momentum conservation in the x-direction and y-direction is,

$$\rho u\frac{\partial u}{\partial x}+\rho v\frac{\partial u}{\partial y}=\frac{\partial}{\partial x}\left(\mu\frac{\partial u}{\partial x}\right)+\frac{\partial}{\partial y}\left(\mu\frac{\partial u}{\partial y}\right)-\frac{\partial P}{\partial x}+S_x \tag{6}$$

$$\rho u\frac{\partial v}{\partial x}+\rho v\frac{\partial v}{\partial y}=\frac{\partial}{\partial x}\left(\mu\frac{\partial v}{\partial x}\right)+\frac{\partial}{\partial y}\left(\mu\frac{\partial v}{\partial y}\right)-\frac{\partial P}{\partial y}+S_y \tag{7}$$

The two-dimensional scalar transport equations for more than one species is

$$u\frac{\partial m_i}{\partial x}+v\frac{\partial m_i}{\partial y}=\frac{\partial}{\partial x}\left(D_{iB}\frac{\partial m_i}{\partial x}\right)+\frac{\partial}{\partial y}\left(D_{iB}\frac{\partial m_i}{\partial y}\right)+S_i \tag{8}$$

A two-dimensional rectangular geometry is generated using commercial CFD package ANSYS. The solution domain was identical to the experimental setup of [40]; i.e. (l x h) 255mm x 1mm, and was used to verify the modeling assumptions and permeation flux model. The domain consisted of 12 x 10^5 hexahedral cells with an average cell size of 0.005 mm. The membrane boundary has an inflated mesh layer with a growth factor of 1.2, having a higher density of cells the boundary growing away towards the bulk. The grid dependency was checked with and without the inflation of mesh layers at the membrane boundary. It was observed for cases without the inflated membrane boundary mesh the solutions diverge early and for cell sizes too small in proportion to the average mesh size of 0.005 mm, the solutions also diverged. Figure 3 shows an enlarged section at the membrane boundary layer. The inflated layers are mesh cells compressed near the boundary to capture the wall effects. The estimation of the boundary layer thickness is essential for the estimation of the solute wall concentration which is then used to calculate the true rejection and the solvent flux and in determining the hydrodynamics inside the membrane channel.

The distance between the adjacent walls at the membrane boundary must be set to be very small length-scales for the scalar estimation in the laminar boundary layer which is prerequisite for film theory, the boundary thickness, δc = 2.5 x 10-7 m was used [40]. The effect of the solute on the solution viscosity and diffusivity were tested in simulations and were found to be insignificant. Hence their effects were approximated to be absent. Experimentally, the diffusivity of ethanol and methanol are similar and the concentrations of Ibuprofen were small to change the overall solution density, diffusivity and viscosity. Hence the numerical approximations were consistent with the experimental observations.

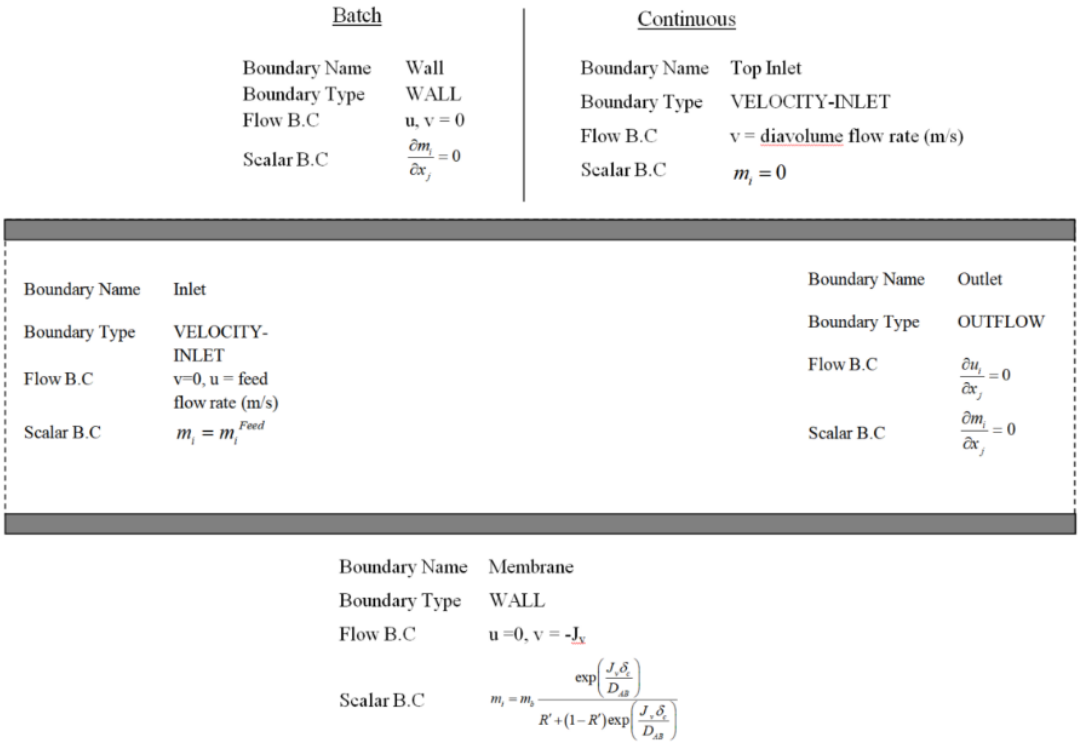

Figure S21. Simulation boundary conditions for the channel geometry

The boundary conditions are shown in Figure 4. The domain consists of the inlet, outlet, membrane boundary and wall. The inlet face is defined as a velocity inlet boundary, whereas the outlet is defined as an outflow boundary. The transmembrane pressure is defined in a macro coupled along with the flow model. The top surface is defined as an impermeable wall; however, the top surface has a zero-slip velocity. The membrane wall is treated as an impermeable wall that doesn't allow any material to pass through, in this way a velocity outlet boundary conditions cannot be specified here. In order to accommodate for the selective permeation through the membrane, the solution permeability and solute permeability flow rates are defined through equations 15 and 16 respectively in Section 4.1.1 in the Supporting Information. In the geometry, the cells adjacent to the defined membrane are specified to have a negative Y velocity to account for the permeation flow into the membrane and away from the mean flow region and to account for the loss of material, sink term are defined proportional to the membrane surface area and as a function of their

respective permeation flow rates as defined in equations 18 and 19 in Section 4.1.1. The fluid is modeled as a laminar flow and two scalar transport equations are solved as the solute and API within the domain of analysis.

4.1.1 Theoretical analysis of concentration polarization

A balance of the convective flux of the solute with the solvent towards the membrane, through the membrane and the flux due to back diffusion of the solute in the bulk of the solution through a 'stagnant film' of film thickness δ can be written as

$$J_W C_P = J_W C - \left(-D \frac{dC}{dz} \right) \tag{9}$$

Integrating equation (9) with the limits

$$\begin{aligned} z = 0, \quad C = C_m \\ z = \delta, \quad C = C_b \end{aligned} \tag{10}$$

where δ is the boundary layer thickness at the membrane surface, with C_b, the concentration of the solute in the bulk solution and C_m, the concentration of the solute at the membrane surface, yields

$$\ln\left(\frac{C_m - C_p}{C_b - C_p} \right) = \frac{J_w \delta}{D} \quad \Rightarrow \quad \frac{C_m - C_p}{C_b - C_p} = \exp\left(\frac{J_w}{k_L} \right) \tag{11}$$

where $k_L=(D/\delta)$ is the liquid-phase mass transfer coefficient at the membrane surface.

Defining the rejection coefficient (also called the fractional coefficient or fractional retention) of the solute as

$$R' = \left(1 - C_p / C_m \right) \tag{12}$$

equation (11) becomes

$$\frac{1 - \left(C_p / C_m \right)}{\left(C_b / C_m \right) - \left(C_p / C_m \right)} = \exp\left(\frac{J_w}{k_L} \right) \Rightarrow \frac{R'}{\left(C_b / C_m \right) - \left(1 - R' \right)} = \exp\left(\frac{J_w}{k_L} \right) \tag{13}$$

rearranging equation (13)

$$\left(C_m / C_b \right) = \frac{\exp\left(J_w / k_L \right)}{R' + \left(1 - R' \right) \exp\left(J_w / k_L \right)} \tag{14}$$

4.1.2 Theoretical model for solvent and solute transport

The transport equations for the components through a nanofiltration membrane consist of two components: the diffusion components and the convection component. For a single solute aqueous solution the solute retention can be described by three transport coefficients (i) specific hydraulic permeability, L_p (ii) local solute permeability, P_s (iii) reflection coefficient σ. The Spiegler-Kedem-Kachalsky (SKK) model states that the fluxes of solute and solvent are directly related to the chemical potential differences between the two sides of the membrane[S1]. The SKK model makes the following assumptions

(i) Predicts the transport of solute and solvent, regardless of the type of solute, solvent and membrane
(ii) The pressure and concentration gradients are the driving forces
(iii) Solute present in the system is semi-permeable to the membrane
(iv) In the concentration polarization layer thickness, the solute has a value that is independent of the diffusion and mass transfer coefficient
(v) L_p, P_s, and σ are constants across the membranes

The fluid and solute mass changes adjacent to the membrane surface with permeation are solved numerically, while the flow and mass transfer through the membrane are solved theoretically, the simplified of the model transport equation can be written as [S2]

$$J_v = L_P\left\{(p_f - p_p - (\Delta\pi_f - \Delta\pi_p)\right\} \tag{15}$$

$$J_{s_i} = P_s(m_f - m_p) - (1-\sigma)m_{s_i}J_v \tag{16}$$

Subscripts *f* and *p* denote the feed and permeate sides respectively while the subscript *i* denotes the i^{th} solute. The observed rejections can be explained by the SKK theory as

$$R_{observed} = \frac{\sigma(1-F)}{1-\sigma F}$$
$$F = \exp\left(-\frac{1-\sigma}{P_s}J_v\right) \tag{17}$$

A theoretically calculated value of the solute mass fraction is calculated at the membrane surface to estimate the values of the permeation flux for the fluid and the solute. The mass permeating through the membrane is modeled using source terms in the continuity and scalar transport equations. The source terms are given as follows

$$S_{vi} = -\frac{(J_v\rho_0 A_i)}{V_i} \tag{18}$$

$$S_{si} = -\frac{(J_s\rho_s A_i)}{V_i} \tag{19}$$

V_i is the cell volume and A_i is the face adjacent to the membrane surface. The source terms allow for the permeation through the membrane boundary even though it's treated as an impermeable wall.

4.1.3 Numerical methods and computational solution

The two-dimensional rectangular channel was solved numerically using the commercial CFD package ANSYS, Fluent which employed the finite volume method to discretize the solution domain into 12 x 10^5 hexahedral cell volumes with an average cell size of 0.005 mm. The higher order scheme (QUICK) was used for the discretization of the convective terms whereas the diffusive terms were discretized using the higher order central differencing scheme (CDS). The SIMPLE algorithm was employed for the coupling of the pressure and velocity terms. Two scalar transport equations are solved along with the fluid equations for the estimation of the solute transport within the domain. The flow is solved as a laminar flow in steady state with user defined macros to implement the scalar mass at the membrane surface and hence estimate the polarization

layer and the permeate flux, all three are circularly linked with the solution thereby estimating all values dynamically. The criterion for convergence was set to 10^{-16} and flow equations were solved until a steady flow developed at the outlet.

The numerical simulations are supported by experimental data. The pure solvent permeability is determined using Darcy's equation (i.e. Eqn 20), the pure solvent flux is estimated experimentally for the operating transmembrane pressure in the membrane channel.

$$J_v = L_p \Delta P$$
$$L_p = \frac{\left(J_v\right)_{\text{experimental}}}{\Delta P} \tag{20}$$

The pure solute permeability is estimated experimentally which is then used in equation (13) to estimate the reflection coefficient; the reflection coefficient is a measure of the extent to which a solute is hindered in its convective flow through the membrane pores. Rearranging equation (18) in terms of the feed and permeate side concentrations we have

$$\frac{C_p}{C_f - C_p} = \frac{1-\sigma}{\sigma} + \frac{P_s\left(C_f - C_p\right)}{\sigma}\frac{1}{J_v} \tag{21}$$

Hence a plot of $C_p/(C_f-C_p)$ vs $1/J_v$ would give a straight line with slope $P_s(C_f-C_p)/\sigma$ and intercept $(1-\sigma)/\sigma$. The initial starting fractional solute retention factor is determined from the experiment using equation (14) and then the true rejection accounting for the influence of the concentration polarization layer on the pressure differential osmotic transmembrane pressure is dynamically calculated using equation (17) in the simulation using a macro. The effect of reverse osmosis on the driving transmembrane pressure is insignificant for large molecules (e.g. BVA, blue dextrin and other protein molecules) [S3], hence the following assumption is made for the solute flux. Equation (22) is representing the solute flux at the membrane

$$J_s = J_v C_m (1 - R') \tag{22}$$

Using the simplifying assumptions, a membrane channel was simulated for a large macromolecule (solute/ impurity) and the much smaller and permeable molecule (API). The outcomes of the simulation are discussed in the next section.

References

S1. A.M. Hidalgo, G. León, M. Gómez, M.D. Murcia, E. Gómez and J.L. Gómez, *Desalination*, 2013, **315**, 70.

S2. T. Ishigami and H. Matsuyama, *Ind. Eng. Chem. Res.*, 2015, **54**, 1665.

S3. B.K. Dutta, Principles of Mass Transfer and Separation Process, PHI Learning Private Limited, 2002.

Table S1 : Tabular Categorization of different mixer designs

	CS3D					CS2D		
	30, 45, 60,	90	120	Tri	Rect	SMX	Kinecs	Serpentine
Permeation Flux	High	Low	Low	High	Moderate	Highest observed amongst CS2D	Good	Good
Susceptibility to Polarization	Low	Low	High	Low	Low	Low	Low	Low
Flow Recirculation	Low	Low	Poor	Poor	Poor	Extremely Good	Extremely Good	Moderate
Preconcentration	High	High	Low	Low	Low	Absent	Absent	Absent
Segmentation	Moderate	Moderate	Absent	Absent		High	Moderate	Extremely Good; eaxh segment behaves like another diafiltration step
Expected Mixedness	Low	Poor	Poor	Good	Ok	Excellent	Excellent	Ok